Downstream development during South African cut-off low development

Thando Ndarana[a,*], Tsholanang S. Rammopo[a], Mary-Jane Bopape[b], Chris J. C. Reason[c], Hector Chikoore[d]

[a] *Department of Geography, Geoinformatics and Meteorology, University of Pretoria, Hatfield, South Africa*
[b] *Department of Research and Innovation,South African Weather Service, Centurion, South Africa*
[c] *Department of Oceanography, University of Cape Town, Cape Town, South Africa*
[d] *Unit for Environmental Sciences and Management, North-West University, Vanderbijlpark, South Africa*

Abstract

Using 39 years of ECMWF renalysis data, an established energetics framework and simple composite analysis this study has shown that South African cut-off low (COL) pressure systems are preceded by downstream development of a baroclinic wave. The upstream eddy kinetic energy, which is associated with the midlatitude jet streak, develops and reaches its maximum before the formation of the closed COL cyclonic circulation. The downstream eddy kinetic energy centre maximises at the point which the closed circulation forms. The upstream eddy kinetic energy centre grows from baroclinic conversion from eddy available potential energy to eddy kinetic energy, whilst the latter grows by receiving energy by means of ageostrophic geopotential fluxes that transport eddy kinetic energy in a north-eastward direction from the upstream centre. These ageostrophic geopotential fluxes are induced, increased in magnitude and directed by processes associated with RWB on the midlatitude dynamical tropopause. and so the downstream energy transfer connects South African COLs to midlatitude processes. The study has further shown that the baroclinic kinetic energy configuration previously associated with wet seasons over South Africa is consistent with times when COLs forms over the country. This study shows further that these two branches are linked by the ageostrophic geopotential fluxes, for COLs that occur in the western half of South Africa.

Keywords: Downstream development, cut-off lows, eddy kinetic energy

*Correspondence: thando.ndarana@up.ac.za

Highlights

Downstream development during South African cut-off low development

Thando Ndarana, Tsholanang S. Rammopo, Mary-Jane Bopape, Chris J. C. Reason, Hector Chikoore

- The study has shown that South African cut-off low (COL) pressure systems are preceded by downstream development.
- Downstream development in the context of the COLs provides a framework to show that the eddy kinetic energy associated with COL formation is transferred from the midlatitudes, is not converted from eddy available potential energy via baroclinic conversion.
- Breaking Rossby waves in the midlatitudes induce and enhance the ageostrophic geopotential fluxes that make the transfer of energy from the midlatitudes to the subtropics possible.

Graphical Abstract

Downstream development during South African cut-off low development

Thando Ndarana, Tsholanang S. Rammopo, Mary-Jane Bopape, Chris J. C. Reason, Hector Chikoore

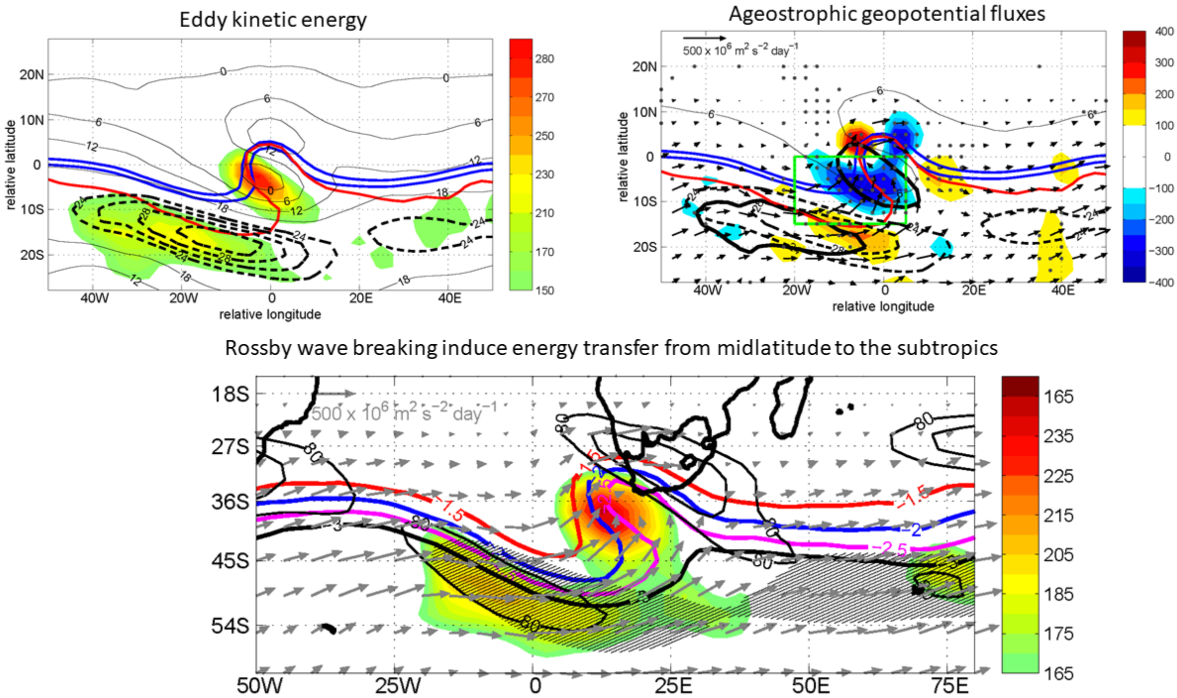

1. Introduction

A cut-off low (COL) pressure system is a closed and cold cored upper tropospheric cyclonic circulation that has been detached from the westerlies (Palmén and Newman, 1969; Pinheiro et al., 2017, 2019) on the anticyclonic barotropic shear side of the jet core (Thorncroft et al., 1993). This closed circulation is induced by high potential vorticity (PV) anomalies (Hoskins et al., 1985) that may be brought about by the equatorward isentropic transport of stratospheric air by means of Rossby wave breaking (RWB) processes (Ndarana and Waugh, 2010; Reyers and Shao, 2019; Barnes et al., 2000a). McIntyre and Palmer (1983) defined RWB as the rapid and irreversible deformation of PV contours that turn back on themselves such that the meridional gradient of the PV is reversed. Such a reversal is most clearly seen when PV is presented on isentropic surfaces (Hoskins et al., 1985. Other studies have defined RWB as overtuning isentropic contours on iso-PV surfaces (e.g. Berrisford et al., 2007) and as the deformation of absolute vorticity on isobaric surfaces (Barnes and Hartmann, 2012). The fact that the closed COL circulation is induced by these anomalies means that its dynamical onset is an upper tropospheric process, but may extend to the lower levels of the atmosphere (Barnes et al., 2020a, 2020b; Portmann et al., 2020) and may induce surface cyclogenesis (Portman et al., 2020). When COLs extend to the surface they may lead to storm surge that can potentially cause extensive damage along the coastal areas in the South African domain (Barnes et al., 2020b).

COLs in the South African domain have been extensively studied using reanalysis products (e.g. Singleton and Reason, 2007a; Favre et al., 2012, 2013) and using numerical models e.g. Singleton and Reason, 2006, 2007a), and have clearly been shown to bring rainfall to different parts of the country (Molekwa et al., 2014; Engelbrecht et al., 2015; Omar and Obiodun, 2020). The typically heavy rainfall associated with COLs implies that east of the upper air trough axis substantial upward motion exists. This vertical uplift is a well known dynamical characteristic of a fully developed baroclinic weather system, with convergence at the surface and divergence aloft. Such a system dissipates when the upper level disturbance catches up with the one at the surface so that its vertical structure becomes equivalent barotropic. Therefore, when

COLs reach South Africa as rainbearing systems; they are usually already matured synoptic weather systems, at least from a dynamic meteorology point of view. To support this notion, given the fact that the COLs are preceded by RWB (Ndarana and Waugh, 2010; Reyers and Shao, 2019), as already mentioned, Favre et al. (2013) and Omar and Obiodun (2020) consistently note that they develop from unstable Rossby waves and, due to this instability, these waves eventually evolve into non-linear regimes and break. This breaking is actually a dissipative process (Methven et al., 2005) during baroclinic life cycles. When viewed in the context of an idealised experiments (e.g. Thorncroft et al., 1993; Kunz et al., 2009; Kunkel et al., 2011), irreversible deformation of the PV contours that signals RWB occurs during the downturn of eddy kinetic energy (K_e), when the vertical propagation of wave activity has ceased and its meridional component dominates. This happens during the barotropic conversion stage and the K_e decreases, as it is converted into mean kinetic energy.

Approaches that have been taken to study COLs in the South African domain have so far focused on processes from the formation of the closed circulation and subsequent impacts, even though linkages with low frequency atmospheric oscillations and remote drivers have been considered (Singleton and Reason, 2007a; Favre et al., 2012) and boundary conditions, Singleton and Reason (2006, 2007b) simulated COLs over South Africa using MM5 and analysed the contribution of SSTs, surface latent fluxes and topography to the evolution of the COL and its associated rainfall. A key outstanding question that warrants analysis is what happens dynamically on days leading up to the formation of the closed circulation.

The connection between COL pressure systems and RWB then suggests that the former may also be viewed in the context of a baroclinic wave life cycle using the energetics framework. For example, Gan and Piva (2013, 2016) employed the Orlanski and Katzfey (1991) system of local energy equations to study the evolution of southeastern Pacific COL pressure systems. They showed that COLs were associated with two K_e centres of differing spatial extent, with the larger one coinciding with the jet streak identified in Ndarana and Waugh (2010), Reyers and Shao (2019). Aspects of the evolution of the jet streak were explained in Ndarana et al. (2020). Based on the Gan and Piva (2013) case study, K_e is then transported from the jet stream via ageostrophic geopotential fluxes into the closed circulation region. However whether this is the case in the South African domain and the cause of the increase in the strength (and perhaps even the onset) of this energy transport in South African COL pressure systems remains an open question.

Tennant and Reason (2005) showed that kinetic energy plays a role in regulating rainfall variability over South Africa. They found that during the wet seasons, the baroclinic kinetic energy breaks into two branches, with one branch located in the subtropics and another in the midlatitudes. They considered these energetics issues of South African rainfall at the seasonal time scale, thus providing a framework within which the questions raised above could be considered. One of the hypotheses that the current study explores is that there could be a midlatitude/subtropical baroclinic kinetic energy transfer that is characterised by the ageostrophic geopotential fluxes, even though there is no theoretical framework that we are aware of that links the Orlanski and Katzefey (1991) and Wiin-Nielson (1962) energetics frameworks (the latter of which was used in Tennant and Reason (2005)).

Given the above, the overall aim of this study is to establish the dynamical processes that take place during the life cycle of South African COLs, assuming that the onset of this life cycle occurs before the closed circulation forms. This study will also link the energetics of COLs to the Tennant and Reason (2005) result. As these are high impact weather systems, such an analysis has the potential for contributing to improving their predictability, particularly at the medium range forecasting time scale. The rest of the paper is organised as follows: In the next section the data and methods are presented. The results Section 3 is divided into subsections that discuss aspects of the dynamical evolution of COLs. Section 4 presents the concluding remarks.

2. Data and methods

2.1. Data

As in Barnes et al. (2020a) and Ndarana et al. (2020), we identify COLs on the 500 hPa isobaric level using the European Centre for Medium-Range Weather Forecasting (ECMWF) Renalysis Interim (ERA-I; Dee et al., 2011). In this diagnostics study, the geopotential height, the three components of the wind and temperature fields were extracted for calculating the mathematical quantities described below. The study covers the years 1979 to 2018 because prior to 1979, reanalysis datasets were unreliable in the Southern Hemisphere (Tennant, 2004) as the data would pre-date the advent of satellite observations and the assimilation thereof into global data assimilation systems.

2.2. Methods

2.2.1. COL Detection and composite analysis

The method for identifying COLs and calculating the composites have been described in Barnes et al. (2020a) and Ndarana et al. (2020), and only a brief description of it is outlined here. It is an 8-step algorithm that starts by identifying closed contours on the 500 hPa geopotential height field. Centres of these closed contours that are north of 15°S and south of 50°S are excluded. To ensure that the circulation around the contour is cyclonic, geopotential heights at the centres are then assumed to be lower than 6 of the immediately surrounding grid points. Once this condition has been been complied with, it is further required that the zonal component of the wind south of the centre be negative to ensure that a cut-off has occurred.

As a fifth step, the cold core condition is imposed, after which all concentric contours are grouped together. These are defined as all closed contours whose centres are within a $10° \times 10°$ grid box. The centre with the lowest 500 hPa geopotential height value is considered to be the final COL centre point. In the final step, COL centres that lie within 1000 km from one another on consecutive time steps are considered to belong to the same evolving COL. As in Singleton and Reason (2007a), we retain only those systems that have a 24 hour duration or longer within the domain bounded by

10 - 40°E longitude and 20 - 40°S latitude.

As in Ndarana et al. (2020), we use the centre of the COL as a reference point when calculating the composite means. Firstly all the fields bounded by a 100° longitude - 50° latitude box, with the middle most point of the box being the COL point are extracted from each field. We then bring these together, so that the middle most points of the fields coincide and then calculate simple means of the fields. No assumption is made except the fact that a closed circulation has formed. It thus follows that the fields that emerge are representative of the COLs. The statistical significance is calculated using the approach of Brown and Hall (1999).

2.3. Diagnostics

To generate the local energetics fields that evolve in space and time, we assume a basic state flow defined by the 31-day time mean (Orlanski and Katzfey, 1991; Lackmann et al., 1999; Danielson et al., 2006) centred on the day of the COL events and the perturbations are the deviations from that time mean. The choice of the 31-day time mean basic state flow leads to simpler equations and Lackmann et al. (1999) suggested that low frequency basic state flow does not significantly influence the energy budget analysis results. The total variables are then decomposed as follows:

$$\mathbf{U} = \mathbf{U}_m + \mathbf{u} \tag{1}$$

$$\mathbf{V} = \mathbf{V}_m + \mathbf{v} \tag{2}$$

$$\Phi = \Phi_m + \phi \tag{3}$$

$$\Theta = \Theta_m + \theta \tag{4}$$

where the capital letters/Greek symbols with no subscript m and with the subscript m represent the total and time mean variables, respectively. The lowercase symbols represent the perturbation fields and $\mathbf{U} = U\mathbf{i} + V\mathbf{j} + \omega\mathbf{k}$ is the three dimensional velocity flow and $\mathbf{V} = U\mathbf{i} + V\mathbf{j}$ is the horizontal flow on isobaric surfaces. The symbols Φ and Θ are the geopotential and potential temperature, respectively.

We employ the flux form of the Orlanski and Katzfey (1991) and Danielson et al.

(2006) eddy available potential energy (P_e) equation given by

$$\partial_t P_e = -\nabla_p \cdot (\mathbf{V} P_e) - \partial_p(\omega P_e) + \omega\alpha + \frac{\alpha_m}{2\Theta_m}\frac{1}{d\widehat{\Theta}/dp}(\mathbf{v}\theta \cdot \nabla_p \Theta_m) + S \qquad (5)$$

where α is the specific volume and the other terms have been defined above. The subscript p in the gradient operator means that it is evaluated whilst keeping pressure constant. As in Orlanski and Sheldon (1993), the correlation between the perturbation temperature and the time mean temperature advection by the eddies as well as other terms that materialised when transforming the advection form of the equation to the flux version of it are all included as non-conservative sources and sinks of P_e, which are represented by S in Eq (5). The form of P_e used in this study is

$$P_e = -\left(\frac{\alpha_m}{2\Theta_m}\frac{1}{d\widehat{\Theta}/dp}\right)\theta^2 \qquad (6)$$

and the hat over Θ represents the horizontal average. The first two terms on the right hand side of Eq. 5 are the horizontal and vertical eddy available potential energy flux terms, the third term is the baroclinic conversion of P_e to K_e and the fourth term represents the conversion from mean available potential energy (P_m) to P_e

McLay and Martin (2002) derived the flux form of the Orlanski and Katzfey (1991) eddy kinetic equation. Here the zonal and meridional momentum correlation, the vertical flux divergence of the rate of work by aerodynamic stress and the curvature terms are all incorporated in the residual term as was the case above, to obtain

$$\partial_t K_e = -\nabla_p \cdot (\mathbf{V} K_e) - \partial_p(\omega K_e) - \mathbf{v} \cdot \nabla_p \phi + [\mathbf{v} \cdot (\mathbf{u} \cdot \nabla)\mathbf{V}_m] + \text{Residual} \qquad (7)$$

which is the K_e equation and $K_e = \mathbf{v} \cdot \mathbf{v} \times 0.5$

Orlanski and Katzfey (1991) decomposed the K_e generation term $-\mathbf{v} \cdot \nabla_p \phi$ as follows

$$-\mathbf{v} \cdot \nabla_p \phi = -\omega\alpha - \nabla_p \cdot (\mathbf{v}\phi)_a - \partial_p(\omega\phi) \qquad (8)$$

The first term in Eq. 8 ($-\omega\alpha$) is the same as the third term in Eq. 5 but with opposite sign, thus confirming it as a conversion term between the two energy forms. This term also materises in the contest of the highly idealised two layer model (see Holton and Hakim, 2014) and takes the form $\overline{\omega_2\psi_T}$, where ψ_T is the baroclinic perturbation streamfunction and the overline represents the zonal average over a wavelength of an idealised baroclinic wave. As in Orlanski and Sheldon (1993), we assume a variable f so that

$$(\mathbf{v}\phi)_a = \mathbf{v}\phi - \mathbf{k} \times \nabla \left(\frac{\phi^2}{2f(y)} \right) \tag{9}$$

which is the ageostrophic geopotential flux. It follows then that K_e is generated by two processes, namely (a) baroclinic conversion (first term in Eq. (8)), which is caused by vertical eddy heat fluxes and (b) ageostrophic flux convergence (second term on Eg. (8)). This system of energy equations was then used by Orlanski and Sheldon (1995) to describe downstream development, involving two energy centres, one upstream and the other downstream, during which K_e is moved by means of energy fluxes ($\nabla_p \cdot (\mathbf{V}K_e)$), whilst the upstream centre radiates energy downstream into the centre to the east of it by means of the ageostrophic geopotential fluxes in Eq. (9).

In their study of the associations between the global energy cycle and South African rainfall, Tennant and Reason (2005) employed a different energetics framework from the one discussed above. Following Wiin-Nielson (1962), Tennant and Reason (2005) decomposed kinetic energgy into barotropic and baroclinic components, defined as $K_{BT} = \mathbf{V}_{BT} \cdot \mathbf{V}_{BT} \times 0.5$ and $K_{BC} = \mathbf{v}_{BC} \cdot \mathbf{v}_{BC} \times 0.5$, respectively. $\mathbf{V}_{BT}$ is the vertically integrated horizontal flow and $\mathbf{v}_{BC} = \mathbf{V} - \mathbf{V}_{BT}$. All the results shown below are pressure-weighted vertical average of the diagnostics.

3. Results

3.1. Eddy available potential energy budget

Classical energetics theory (Lorenz, 1955) states that the P_m in the atmosphere is generated by diabatic processes, but converted to P_e, and then to K_e by means of baroclinic processes, which are dynamical in nature. This sequence of events dictates that we discuss the P_e budget, using Eq. 5, associated with COLs first and then proceed to that of K_e in the subsequent subsections. Fig. 1 (a) to (e) shows the composite evolution of P_e (see Eq. 6) that is associated with 48-hour COL events in the domain, relative to the jet streak (Keyser et al., 1985). This jet streak that forms and propagates during the COLs has been reported in several previous studies (Ndarana and Waugh, 2010; Reyers and Shao, 2019; Ndarana et al., 2020). Its eastward translation is caused by the advection of zonal momentum by the zonal flow, whilst the meridional advection of zonal momentum changes its northwest/southeast orientation to become more zonal as it passes the closed circulation (Ndarana et al., 2020). As the jet streak propagates eastward, the P_e centre moves along with it, and it is always located in the diffluence region of the jet streak. It reaches it's maximum at the point when the COLs form and subsequently dissipates beyond that point as the jet streak propagates further eastward. The co-location of the jet streak and P_e is the first indication that, not only does the former bring about the anticyclonic barotropic shear that is necessary for lower stratospheric/upper tropospheric Rossby waves to break (Peters and Waugh, 2003; Ndarana and Waugh, 2010; Bowley et al., 2019) as indicated by the thick red contour in Fig. 1 (a) to (e) that represents the PV = -2 PVU (1PVU = 10^{-6} m^2 s^{-1} K kg^{-1}), it is also a source region for P_e. Because this PV contour represents the dynamical tropopause (Hoskins, 1991) in the midlatitudes, the potential vorticity anomalies that induce the closed COL circulation (Hoskins et al., 1985), demonstrate that there is midlatitude stratospheric air presence where the South African COLs form.

Note that P_e has an approximately oval structure and there are areas of $\partial_t P_e < 0$ ($\partial_t P_e > 0$) at its rear (front) ends. This is shown in Fig. 1(f) to (j) by the blue (yellow to brown) shading located in the western (eastern) half of the thick black contour that represents $P_e = 100$ m^2 s^{-2}. It is interesting to note that the $\partial_t P_e$ field is orientated in the same way as $\partial_t u$ (cf. Fig. 3 in Ndarana et al., 2020) and temporally and spatially coincides with it. Therefore the eastward movement of P_e is dynamically coupled to that of the jet streak. Within the time frame of the COLs considered in this study, the pattern of P_m, P_e conversion terms (not shown), represented by the third term on the right hand side of Eq. 5, coincides with those of $\partial_t P_e$ but with opposite sign. However the combined effect of the two terms (not shown)

$$-\nabla \cdot (\mathbf{V} P_e) + \frac{\alpha_m}{2\Theta_m} \frac{1}{d\widehat{\Theta}/dp} (\mathbf{v}\theta \cdot \nabla_p \Theta_m) \tag{10}$$

produces composite patterns that are similar to those of $-\nabla \cdot (\mathbf{V} P_e)$, that are shown in Fig. 2 (a) to (e). This means that the P_e flux divergence is the more dominant forcing between the two, and effects the eastward propagation of the energy centre in Fig. 1. The fluxes (represented by the arrows in the left panels of Fig. 2) show that the energy is transported from the rear end of the potential energy centre (where there is flux divergence) to the front end of the structure (where there is flux convergence).

The strength and direction of the fluxes is influenced by two factors. The first is the amount of P_e in the jet streak, and the strength of zonal flow of the jet streak itself. The second factor is the direction of the meridional flow, which is poleward (equatorward) at the jet entrance (exit) region, but also weaker than the zonal jet streak flow (Ndarana et al., 2020). This causes the fluxes to be strong in the P_e and weaker everywhere else, and further highlights the reason why the P_e structure follows the jet streak.

The process that links P_e to K_e is baroclinic conversion (Orlanski and Katzfey, 1992; Orlanski and Sheldon, 1993; McLay and Martin, 2002; Decker and Martin, 2005; Harr and Dea, 2009). In Eqs 5 and 7, this process is represented by the term $\omega\alpha$. When $\omega\alpha < 0$, then a conversion from P_e to K_e takes place. Composites of $\omega\alpha$ shown in Fig. 2 (f) to (j) demonstrate that baroclinic conversion during the evolution of South African COLs dominates during the six hourly time steps leading up to the time step at which the systems form at t = 0 hours. These composites also show that it occurs in the rear end of the P_e centre, represented in Fig. 2 by the thick solid contour and is associated with increasing midlatitude baroclinicity as demonstrated by the increasing strength of the jet streak (Ndarana et al., 2020). Note that the relative location of $\omega\alpha < 0$ and $-\nabla \cdot (\mathbf{V} P_e) < 0$ means that $\partial_t P_e < 0$ found in the rear end of the P_e centre is caused by both baroclinic conversion and P_e flux divergence, with the former ceasing earlier and the latter continuing beyond the day of COL formation.

3.2. Downstream development during COL evolution

We now discuss the evolution of K_e (Fig. 3 (a) to (e)) and contrast it with that of P_e (Fig. 1 (a) to (e)) - thus making the case for downstream development that is associated with COL pressure systems. The main difference between the structures of the two energy forms is that the former has two centres; one (the midlatitude K_e centre) located in the confluent region of the midlatitude jet streak and another (referred to as the subtropical K_e centre) develops north east of jet streak, where we find anticyclonic barotropic shear and PV overturning. This places the former upstream and the latter downstream prior to formation of the closed circulation in COLs. We will therefore use the terms "midlatitude K_e centre" and "upstream K_e centre" as well as "subtropical K_e centre" and "downstream K_e centre" interchangeably. In addition, at each time step, P_e has only one centre, always located east (upstream) of the midlatitude K_e centre. After developing, the K_e centres maximize at different times during the evolution of COLs, with the midlatitude K_e doing so first.

When the K_e structures are viewed relative to the jet streak and the closed COL circulation north east of it, they may be seen as two separate entities, because whilst the jet streak influences the COLs, the two are different processes. However, when viewed relative to the composite RWB, which highlights the ridge/trough/ridge system at play, they may be seen as a clear case of downstream development, as described in Orlanski and Sheldon (1995), (cf. their Fig 3). From this point of view, Stage 1 occurs at around t = -36 hours in Fig. 3 (a), when the midlatitude K_e (which corresponds to the western centre in Orlanski and Sheldon (1995)) propagates east, whilst increasing in strength and the upstream centre develops. The saturation of this upstream midlatitude energy centre, whilst the one downstream continues to intensify and approaching its maximum, is a clear signature of stage 2 in a developing baroclinic wave that occurs in Fig. 3(c). Stage 3 occurs at t = 0 hours (Fig. 3(d)), because the western centre has begun to dissipate, whilst the downstream reaches its maximum.

Beyond stage 3, both energy centres dissipate. Composite evolution of COLs of all durations were examined and they exhibit exactly the same behaviour. It follows then that the COLs in the South African domain are preceded by the downstream development of a baroclinic wave.

Similarly to Orlanski and and Sheldon (1995), downstream K_e saturates at higher values than the one up stream. There are, however, important differences between the observations described above and the Orlanski and Sheldon model of downstream development. First the upstream centre is much larger than the one located downstream, which is consistent with the Gina and Piva (2013) COL case. Secondly, the downstream centre appears to be quasi-stationary, relative to the upstream structure - and the the former eventually actually moves past as dissipation occurs. As a result of the relative speed of the two centres, the baroclinic wave has a southwest/northeast orientation so that the trough axis has a northwest/southeast slant, as opposed to that of the Orlanski and Sheldon idealised model, in which the trough axis is parallel to the latitude axis.

To enable a direct comparison with the diagnostics employed by Tennant and Reason (2005), the baroclinic kinetic energy is shown in Fig. 3 (f) to (j). In the midlatitudes, both forms of kinetic energy are placed at more or less the same position relative to the jet core (i.e. in the confluent region of the jet). They also propagate eastward in unison with the streak and saturate at the same time (before the formation of the COL). The difference between the two, though, is that the subtropical energy centre is placed north east of the closed circulation and develops as the small scale jet streak does the same, during the formation of the split jet (Ndarana and Waugh, 2010; Reyers and Shao, 2019; Ndarana et al., 2020). Both centres in the case of baroclinic kinetic energy can thus be considered an artefact of jet streaks, which stands to reason since these are regions of strong low level meridional temperature gradients.

3.3. *The generation and movement of the midlatitude eddy kinetic energy*

The use of Eq. 7, processes that inform the evolution of the two K_e centres will now be explained, by first considering the $\partial_t K_e$ fields. These are the shaded areas in Fig. 4 (a) to (e). As was the case with $\partial_t Pe$, the distribution of $\partial_t K_e$ relative to K_e

centre is such that $\partial_t K_e < 0$ and $\partial_t K_e > 0$ are found at the rear and front ends of the approximately oval K_e shape, respectively. This ensures that the maximum values of K_e, with respect to time, occur where $\partial_t K_e = 0$, which divides the K_e diagonally across, from the north-west to the south-east. These source and sink regions of K_e are consistent with the idealised model of Orlanski and Sheldon (1995).

The source region ahead of the midlatitude K_e centre is, first and foremost, associated with the baroclinic conversion of P_e to K_e. Comparing the corresponding panels in Figs 2 (f) to (j) and 4 (a) to (e) shows that regions of $-\omega\alpha > 0$ cover regions of $\partial_t K_e > 0$ that are slightly upstream. It is important to note at this point that $K_e(P_e)$ is located in the confluent (diffluent) region of the jet streak. This relative position of the energy forms makes sense because energy conversion occurs from P_e to K_e. The baroclinic conversion in the PV overturning region is weak. It is thus of no significance and will not be discussed further.

The source region of the midlatitude K_e centre is secondly impacted or informed by the K_e flux convergence (i.e $-\nabla \cdot \mathbf{V}K_e > 0$). These are shown in Fig. 4 (f) to (j). This field affects $\partial_t K_e > 0$ slightly downstream of the region where P_e is converted to K_e. The rear end of the K_e centre is characterised by divergence and the flux vectors, $\mathbf{V}K_e$, are oriented consistently to this. The fluxes that move energy from the back to the front of the energy centre are of significant size in the middle of the centre, for similar reasons to those that were discussed in Subsection 3.1. Arguments as to how the K_e translates eastward are, thus, similar to those of P_e. Outside the jet streak, in the PV overturning region (close to the closed COL circulation), the eddy kinetic fluxes are oriented in a northward direction and their convergence is mostly concentrated in the upstream end of the subtropical energy centre (eastern energy centre). This phenomenon is most clearly seen from about t = -24 to 0 hours in Fig. 4 (g) to (i). The fact that the energy flux is stronger in the western half of the this K_e centre explains why it is oriented as it is. Its rear (or upstream) end moves further northward as compared to the eastern part. The orientation of the fluxes in the PV overturning region is caused by the fact that the zonal flow is significantly decelerated there to values close to zero and is, in some cases, slightly negative (Ndarana et al., 2020). The direction of the fluxes is consistent with the flux divergence (convergence) that is found on the south (north) end of the subtropical K_e centre.

3.4. The evolution of the subtropical eddy kinetic energy centre

As noted above, baroclinic conversion in the PV overturning region (where the subtropical K_e centre is located, highlighted by the green box in Fig. 5) is small (see Fig. 2 (f) to (j)) and secondly, again as noted above, the K_e fluxes move the centres. It follows then that these two processes cannot be responsible for the generation and growth of the subtropical K_e centre. Instead, its growth comes from receiving energy by means of the ageostrophic geopotential fluxes (left panels Eq. 5) which "radiate" energy from the front end of the midlatitude K_e into its rear end. The exact area in the midlattude centre where the energy originates is indicated by $\nabla_p \cdot (\mathbf{v}\phi)_a > 0$. The notion of radiative energy transfer is used here to distinguish this process from the fluxes (Orlanski and Sheldon, 1995) that were discussed in the previous section, as the two types of fluxes play different roles. These radiative energy transfer processes start developing from t = -48 hours (not shown), progressively evolve and mature through t = -12 hours as they curve more sharply (as the red contour shows the deepening ridge). They appear to reach their maximum strength when the subtropical K_e reaches its maximum on t = +0 hours (Fig. 5 (d)), after which it wanes. The downstream energy centre thus develops and grows by receiving energy from the upstream midlatitude centre via $(\mathbf{v}\phi)_a$.

Simple physical arguments can be used to explain the onset of ageostrophic fluxes, their increase in strength and orientation. The area between the two energy centres (green box) in Fig. 5, characterised also by positive PV anomalies (i.e. the western lobe of the breaking wave), is a ridge and therefore the flow in the region is anticyclonic and supergeostrophic (Lim and Wallace 1991). Therefore, the ageostrophic circulation would also exhibit anticyclonic behaviour (see orientation of the arrows in the left panels of Fig. 5 (f) to (j)). It is important to that the subgeostrophic nature of the flow at the top of the trough, above the area of the closed circulation. This is entirely consistent with our understanding of the behaviour of flow, thus confirming our findings.

Since the highlighted area is a ridge, it follows that $\phi > 0$ (brown shading in the left panels of Fig. 5 (f) to (j)). The flux vectors will have the same direction as the ageostrophic flow and will therefore be directed as shown in the area highlighted by the green box, particularly from t = -24 hours (Fig. 5 (g)) to t = +12 hours (Fig. 5 (j)). As the waves break, the values of ϕ increase in magnitude. This is clearly an effect of the deepening ridge, as tropospheric air is advected anticyclonically and poleward by the wave breaking processes. Therefore the combined effect of increase in the strength of $\mathbf{v}_a$, its direction and the increasing magnitude of ϕ explains the development and increasing strength of $(\mathbf{v}\phi)_a$.

3.5. Linkages of COLs to midltitude processes

Downstream development provides a framework of linking COLs that impact South Africa to midlatitude processes. Given that, we now consider the relationship between the diagnostics presented above in a geographical context of South Africa and attempt to link the results obtained here to those of Tennant and Reason (2005).

Following Singleton and Reason (2007a), we divide the South African domain (see Subsection 2.2) into four subdomains (see Fig 6 (a)), A (red), B (blue), C (green), and D (magenta), that are bounded by (10 - 27°E, 30 - 40°S), (10 - 27°E,20 - 30°S), (27 - 40°E, 20 - 30°S) and (27 - 40°E, 30 - 40°S), respectively. Unlike Singleton and Reason (2007), though, we say that a COL event belongs to the region in which it was first identified, even if it evolves into the downstream (or upstream for that matter). Of the 476 COL cases that were identified in this study, 232 (45%), 107 (21%), 52 (10%) 85 (17%) are found in regions A, B, C and D, respectively. All four regions exhibit a minimum number of COLs during the summer and maximum occurs in October for region A and B, in April for region D and in May for region C.

We now make a case for the notion that the K_e associated with COLs that affect South Africa originates in the midlatitudes. As discussed in Subsection 3.4, the midlatitude K_e propagates eastward with the jet, and as it does, energy is transferred from it by means of ageostrophic geopotential fluxes so that the downstream K_e grows, in strength. In this section we present this result in a geographical setting to show that depending on where the COLs form in the South African domain, the downstream K_e centre will behave differently. For Region A COLs (left panels of Fig. 7) and Region B COLs (right panels of Fig. 7) the downstream K_e centre develops west of 20°E in the South Atlantic Ocean. For both categories of COLs, it remains west of this latitude line and then propagates towards the southwestern tip of Africa. At t = 0 hours, the K_e associated with Region A COLs is eventually located south of the one for Region B and it is stronger. The energy transfer occurs as the midlatitude jet streak propagates eastward and increases in strength, thus bringing with it increasing anticyclonic barotropic shear, and increasing strain rate (Nakamura and Plumb 1994) that leads wave breaking on the 330 K dynamical tropopause in the case of Region A COLs. The wave breaking induces the ageostrophic geopotential fluxes, as shown in Subsection 3.4. Simple experimentation shows that for Region B COLs, the wave breaking that influences the fluxes is most clearly seen on the 340 K isentropic surface. The associated of Region A and B COLs with RWB on the 330 K and 350 K, respectively, explains the t = 0 hours position (Figs 7 (d) and (i)) of the respective K_e centres, relative to one another. The difference in the intensity of the eddy kinetic energy density of the two categories of COLs can also be explained by the RWB. Observing that the PV = -1.5 PVU contour turns back on itself in the case of Region A and not in the case of Region B COLs shows that the fluxes associated with the latter will be weaker and hence the eddy kinetic energy associated with them.

As noted in the Introduction, Tennant and Reason (2005) found that wet South African seasons are associated with two branches of the baroclinic kinetic energy. Fig. 7 shows this split (thin black contours). This figure also shows that COLs that develop in the western half of South Africa are associated with a large scale baroclinic kinetic energy structure that is located over subtropical South Atlantic, South African mainland and South West Indian Ocean, and oriented in a northwest/southeast slant. It is quasi-stationary relative to the one observed to appear to be moving with the midlatitide jet streak.

Fig. 7 suggests that the subtropical baroclinic kinetic energy centre is influenced by midlatitude processes. Even though, to the best of our knowledge, there is no known theoretical framework that unifies the energy equation systems of Wiin-Nielson (1962) and Orlanski and Katzfey (1991), Fig. 7 suggests that the ageostrophic geopotential fluxes might be responsible for the variations of the subtropical baroclinic kinetic energy. The magnitude of the subtropical kinetic increases (decreases) as the fluxes strengthen (weaken) during wave breaking. It appears as though it is influenced by the fluxes that are influenced by the subgeostrophic flow from the west over the South Atlantic Ocean, which are associated with the presence of COLs and RWB in that region. Also the supergeostrophic flow from the south-west (and the increasing $\phi > 0$ discussed in Subsection 3.4) causes the fluxes to be orientated northeastward, into the eastern half of the subtropical baroclinic kinetic energy branch. In this study, we thus propose that the branches of baroclinic kinetic energy of Tennant and Reason (2005) are connected.

The transfer of eddy kinetic energy from the midlatitudes into the eastern parts of the South African domain is facilitated by wave breaking on the 340 K and 330 K dynamical tropopause for Region C and D COLs, respectively. Note that the RWB processes associated with these COLs occur downstream from those shown in Fig. 8 and discussed above. The K_e density associated with Region C COLs is much weaker than its Region D COL counterpart. This is caused by the much weaker ageostrophic geopotential fluxes out of the midlatitudes, as informed by the depth of the tropopause fold associated with them. Observe the behaviour of the PV = -1.5 PVU (thick red contour), which is much more deformed in the case of Region D COLs than in that of Region C COLs. When the deformation of this contour is compared across all categories of COLs (Figs 7(d), (i), 8(d) and (i)), it becomes apparent that the depth of the PV anomaly might be playing a role in the strength of the K_e and might related to the extension of the COLs to the surface (see Barnes et al., 2020). This will be a subject of further analysis because it is beyond the scope of the current study. The weak nature of the Region C COL K_e density and orientation of the associated fluxes means that the COLs that occur in this area have little connections to the midlatitudes, except the fact that the PV anomalies that induce them are a results of wave breaking that is caused by the midlatitude jet.

In stark contrast to Fig. 7, inspection of Fig. 8 indicates that the subtropical baroclinic kinetic energy is located in the Indian Ocean for COLs that develop over the eastern half of the country. For Region D COLs in is more further east than for Region C COLs. Therefore, if there is any connection between the subtropical branch of baroclinic kinetic energy to its midlatitude counterpart, it happens much further downstream and not over South Africa as we have found that to be the case for western COLs. The direction of the fluxes that might influence these subtropical baroclinic energy structures are direction consistently to where they are located. The same applies to ageostrophic geopotential fluxes associated with the subgeostrophic flow leaving subcontinent from southern Mozambique.

4. Concluding remarks

Using 39 years (1979 - 2018) of ECMWF reanalysis data, an established local energetics framework (Orlanski and Katzfey, 1991) and simple composite analysis, this study has shown that South African COL pressure systems are preceded by downstream development of a baroclinic wave (Orlanski and Sheldon, 1995). This process is most clearly seen by examining eddy kinetic energy (K_e), which is converted from eddy available potential energy (P_e) as found in classical energetics theory (Lorenz, 1955). However additional processes are required to be considered to complete the picture that emerges in a spatially varying setting. To summarise the processes involved, we proceed as follows:

1. A few days before the formation of the closed COL circulation, the midlatitude jet streak first propagates in the south eastward direction (by means of momentum advection processes - Ndarana et al., 2020) and then more zonally, whilst gaining in strength. The jet streak propagates together with P_e in its diffluence regions and K_e further upstream in the confluence of the streak.
2. This midlatutide K_e centre grows by gaining energy from the P_e ahead of it by means of baroclinic conversion, which continues up to the point when the closed COL circulation forms and appears to cease thereafter as the jet streaks passes south of the COLs. The movement of the K_e is caused by energy fluxes

by the total flow within the energy centre and they distribute the energy from the rear to front end of the centre. The strength and direction of the fluxes are influenced by the flow of the jet streak in the case of the middlatitude K_e centre.

3. The propagation of the jet streak and its increasing zonal flow, coupled with the smaller scale jet streak north of the COL region, constitute a split jet found in previous studies (Ndarana and Waugh, 2010; Reyers and Shao, 2019), which in turn, increases anticyclonic barotropic shear and shearing strain (Nakamura and Plumb 1994) leading to anticyclonic RWB (Peters and Waugh, 2003), signalled by PV overturning. The wave breaking processes create a ridge southwest of the COL circulation but on the equatorward side the jet and this ridge deepens as wave breaking evolves. As a result the flow becomes increasingly super-geostrophic and the geopotential anomalies deepen, thus inducing ageostrophic geopotential fluxes, and with time, increasing their magnitude. The super-geostrophic flow that is associated with the wave breaking is directed anticyclonically, which in turn informs the direction of the fluxes towards the COL regions because the geopotential perturbations are positive.

4. These ageostrophic geopotential fluxes are responsible for transferring energy from the upstream K_e to the one downstream. Thus the latter grows, not from baroclinic conversion, but from ageostrophic geopotential flux convergence. It then reaches a maximum at the point when the closed COL circulation forms.

Overall, the upstream K_e centre increases, whilst another K_e centre develops downstream. The former reaches its maximum before the formation of the COLs, and the latter continues to grow. By the time the downstream structure reaches a maximum at the point in time that the COLs form, the centre upstream has begun to dissipate. This is a sequence of events that characterises downstream development and the growth and decay of these energy centres are informed by the processes listed above. Therefore COLs do indeed develop from unstable synoptic scale Rossby waves (Favre et al, 2012; Omar and Obiodun, 2020). This is also demonstrated by PV, which evolves to the point of over turning of the PV contour.

This study has shown that COLs that occur over the northwestern, southwestern and southeastern parts of the South African domain, as defined, here have strong links to the midlatitudes. Using the downstream development framework, it was shown that the K_e that is associated with COLs is transferred from the midlatitude by energy radiative processes that are induced and enhanced by wave breaking on the midlatitude dynamical tropopause on different isentropic surfaces. These midlatitude connections during the evolution of dynamical processes leading up to COL formation also appear to connect the subtropical branch of the baroclinic kinetic energy to its midlatitude counter part that were identified by Tennant and Reason (2005). It was shown in that study that when configured in this way, the two centres of baroclinic eddy kinetic energy characterise wet South African seasons. It should be mentioned, however, while the connection between the two baroclinic kinetic energy is clear, it is necessary to quantify it in a future investigation.

Acknowledgements: The authors would like to thanks Michael Barnes for providing the COL cases. The authors would also like to thank Prof Emma Archer for her comments that helped improve the manuscript. This study is funded by the South African Water Research Commission (Grant K5-2829).

References

[1] Barnes, E.A., Hartmann, D.L., 2012. Detection of Rossby wave breaking and its response to shifts of the midlatitude jet with climate change. J. Geophys. Res. 117, D09117, doi:10.1029/2012JD017469.

[2] Barnes, M.A., Ndarana, T., Landman, W.A., 2020a. Cut-off lows in the southern Hemisphere and their extension to the surface. Clim. Dyn. Submitted.

[3] Barnes, M.A., Turner, K., Ndarana, T., Landman, W.A., 2020b. Cape Storm: A dynamical study of a cut-off low and its impact on South Africa. Atmos. Res. Submitted.

[4] Berrisford, P., Hoskins, B.J., Tyrlis, E., 2007. Blocking and Rossby wave breaking

on the dynamical tropopause in the Southern Hemisphere. J. Atmos. Sci. 64, 2881 2898.

[5] Bowley, K.A., Gyakum, J.R., Atallah, E.H., 2019. A New Perspective toward cataloging Northern Hemisphere Rossby Wave Breaking on the Dynamic Tropopause. Mon. Wea. Rev. 147, 409 - 431.

[6] Brown, T.J., Hall, B.L., 1999. The use of t values in climatological composite analyses. J. Climate. 12, 2941 2944.

[7] Danielson, R.E., Gyakum, J.R., Straub, D., 2006. A case study of downstream baroclinic development over the North Pacific Ocean. Part II: Diagnoses of eddy energy and wave activity. Mon. Wea. Rev. 134, 1549 1567.

[8] Decker, S.G., Martin, J.E., 2005. A local energetics analysis of the life cycle differences between consecutive,explosively deepening, continental cyclones. Mon. Wea. Rev. 133, 295 - 316.

[9] Dee, D.P., Uppala, S.M., Simmons, A.J., Berrisford, P., Poli ,P., Kobayashi, S., Andrae, U., Balmaseda, M.A., Balsamo, G., Bauer, P., Bechtold, P., Beljaars, A.C., van de Berg, L., Bidlot, J., Bormann, N., Delsol, C., Dragani, R., Fuentes, M., Geer, A.J., Haimberger, L., Healy, S.B., Hersbach, H., Hlm, E.V., Isaksen, L., Kllberg, P., Khler, M., Matricardi, M., McNally, A.P., MongeSanz, B.M., Morcrette, J., Park, B., Peubey, C., de Rosnay, P., Tavolato, C., Thpaut, J., Vitart, F., 2011. The ERA Interim reanalysis: con guration and performance of the data assimilation system. Q. J. R. Meteorol. Soc. 137, 553 - 597.

[10] Engelbrecht, C.J., Landman, W.A., Engelbrecht, F.A., Malherbe, J., 2015. A synoptic decomposition of rainfall over the Cape south coast of South Africa. Clim. Dyn. 44, (9-10), 2589 - 2607.

[11] Favre, A., Hewitson, B., Tadros, M., Lennard, C., Cerezo-Mota, R., 2012. Relationships between cut-off lows and the semiannual and southern oscillations. Cim. Dy.n 39, (7-8), 1473 - 1487.

[12] Favre, A., Hewitson, B., Lennard, C., Cerezo-Mota, R., Tadross, M., 2013. Cut-off lows in the South Africa region and their contribution to precipitation. Clim. Dyn. 41, 2331 - 2351.

[13] Gan, M.A., Piva, E., 2013. Energetics of a southeastern Pacific cut-off low. Atmos. Sci. Lett. 14,272 - 280.

[14] Gan, M.A., Piva, E.D., 2016. Energetics of southeastern Pacific cutoff lows. Clim. Dyn. 46, 3453 - 3462.

[15] Harr, P.A., Dea, J.M., 2009. Downstream development associated with the extratropical transition of tropical cyclones over the western North Pacific. Mon. Wea. Rev. 137, 1295 - 1319.

[16] Holton, J.R., Hakim, G.J., 2014. An Introduction to Dynamic Meteorology. 5th ed. Elsevier Academic Press, 553 pp.

[17] Hoskin, B.J., 1991. Towards a PV-θ view of the general circulation. Tellus. 43, AB: 27 - 35.

[18] Hoskins, B.J., Mcintyre, M.E., Robertson, A.W., 1985. On the use and significance of isentropic potential vorticity maps. Q. J. R. Meteor. Soc. 111, 877 - 946.

[19] Keyser, D., Shapiro, M.A., 1986. A review of the structure and dynamics of upper level frontal zones. Mon. Wea. Rev. 114, 452 - 499.

[20] Kunkel, D., Hoor, P., Wirth, V., 2016. The tropopause inversion layer in baroclinic life-cycle experiments: the role of diabatic processes. Atmos. Chem. Phys. 1,, 541 - 560.

[21] Lackmann, G.M., Keyser, D., Bosart, L.F., 1999. Energetics of an intensifying jet streak during the Experiment on Rapidly Intensifying Cyclones over the Atlantic (ERICA). Mon. Wea. Rev. 127, 2777 2795.

[22] Lim, G.H., Wallace, J.M., 1991. Structure and evolution of baroclinic waves as inferred from regression analysis. J. Atmos. Sci. 48, 1718 - 1732.

[23] Lorenz, E.N., 1955. Available potential energy and the maintenance of the general circulation. Tellus. 7, 157 167.

[24] Methven, J., Hoskins, B.J., Heifetz, E., Bishop, C.H., 2005. The counter-propagating Rossby-wave perspective on baroclinic instability Part IV: Nonlinear life cycles. Q. J. R. Meteorol. Soc. 131, 1425 1440.

[25] McIntyre, M.E., Palmer, T.N., 1983. Breaking planetary waves in the stratosphere. Nature. 305, 593 600.

[26] McLay, J.G., Martin, J.E., 2002. Surface cyclolysis in the North Pacific Ocean. Part III: Composite local energetics of tropospheric-deep cyclone decay associated with rapid surface cyclolysis. Mon. Wea. Rev. 130, 2507 - 2529.

[27] Moelekwa, S., Engelbrecht, C.J., deW Rautenbach, C.J., 2014. Attributes of cut-off low induced rainfall over the Eastern Cape Province of South Africa. Theor. Appl. Climatol. 118, (1-2), 307 - 318.

[28] Nakamura, M., Plumb, R.A., 1994. The effects of flow asymmetry on the direction of Rossby wave breaking. J. Atmos. Sci. 51, 2031 - 2045.

[29] Ndarana, T., Rammopo, T.S. Chikoore, H., Barnes, M.A., Bopape, M., 2020. A quasi-geostrophic diagnosis of cut-off low pressure systems over South Africa and surrounding ocean. Clim. Dyn. In press.

[30] Ndarana, T., Waugh, D.W., 2010. The link between cut-off lows and Rossby wave breaking in the Southern Hemisphere. Q. J. R. Meteor. Soc. 136, 869 - 885.

[31] Omar, S.A., Abiodun, B.J., 2020. Characteristics of cut-off lows during 2015-2017 drought in the Wester Cape, South Africa. Atmos. Res. 235, (2020) 104772.

[32] Orlanski, I., Katzfey, J., 1991. The life cycle of a cyclone wave in the Southern Hemisphere. 1. Eddy energy budget. J. Atmos. Sci. 48, 1972 - 1998.

[33] Orlanski I and Sheldon J (1993) A case of downstream baroclinic development over western North America. Mon Wea Rev, 121: 2929 - 2950.

[34] Orlanski, I., Sheldon, J.P., 1995. Stages in the energetics of baroclinic systems. Tellus. 47A, 605 - 628.

[35] Peters, D., Waugh, D.W., 2003. Rossby wave breaking in the Southern Hemisphere wintertime upper troposphere. Mon. Wea. Rev. 131, 2623 - 2634.

[36] Palmén, E., Newtown, C.W., 1969. Atmospheric circulation systems, their structure and physical interpretation. Academic Press.

[37] Pinheiro, H.R., Hodges, K.I., Gan, M.A., 2019. Sensitivity of identifying cut-off lows in the Southern Hemisphere using multiple criteria: implications for numbers, seasonality and intensity. Clim. Dyn. 53, 6699 - 6713.

[38] Pinheiro, H.R., Hodges, K.I., Gan, M.A., Ferreira, N.J., 2017. A new perspective of the climatological features of upper level cutoff lows in the Southern Hemisphere. Clim. Dyn. 48, 541 - 559.

[39] Reyers, M., Shao, Y., 2019. Cut off lows off the coast of the Atacama Desert under present day condition and in the Last Glacial Maximum. Glob. Plan. Change. 181, 102 - 983.

[40] Singleton, A.T., Reason, C.J.C., 2006. A numerical model study of an intense cut-off low pressure system over South Africa. Mon. Wea. Rev. 135, 1128 - 1150.

[41] Singleton, A.T., Reason, C.J.C., 2007a. Variability in the characteristics of cut-off low pressure systems over subtropical Southern Africa. Int. J. Climatol. 27, 295 - 310.

[42] Singleton, A.T. and Reason, C.J.C., 2007b. A numerical model study of an intense cut-off low pressure system over South Africa. Mon. Wea. Rev., 135, 1128-1150.

[43] Tennant, W.J., 2004. Considerations when using pre-1979 NCEP/NCAR reanalysis in the southern hemisphere. Geophys. Res. Lett. 31: L11112.

[44] Tennant, W.J., Reason, C.J.C., 2005. Associations between the Global Energy Cycle and Regional Rainfall in South Africa and Southwest Australia. J. Climate. 18, 2032 - 3047.

[45] Thorncroft, C.D., Hoskins, B.J., McIntyre, M.E., 1993. Two paradigms of baroclinic-wave life-cycle behaviour. Q. J. Roy. Meteor. Soc. 119, 17 - 55.

[46] Wiin-Nielsen, A., 1962. On transformation of kinetic energy between the vertical shear flow and the vertical mean flow in the atmosphere. Mon. Wea. Rev. 90, 311 322.

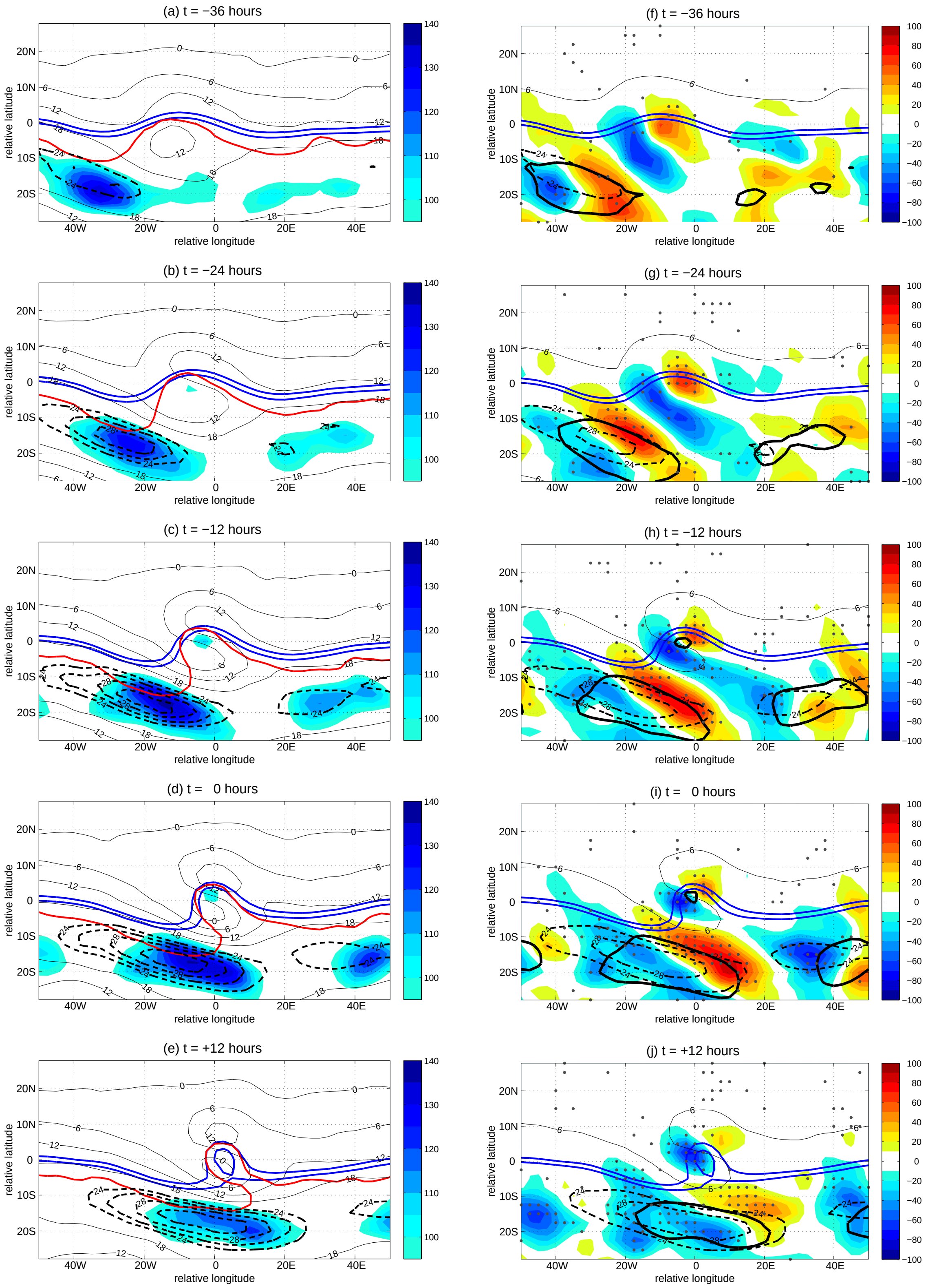

Figure 1: Time-lagged composites of vertically integrated eddy available potential energy (shaded in blue) shown on the left panels. The eddy available potential energy is plotted from 95 - 140 m^2 s^{-2}. The thick red contour is the -2 PVU contour on the 330 K isentropic surface. The right panels show time-lagged composites of the tendency of vertically averaged eddy available potential energy (shaded) plotted in m^2 s^{-2} day^{-1}. In all panels, the thick blue contours are the 5614 and 5635 gpm geopotential height. The thin black contour is the 6 m s^{-1} zonal isotach and the thick dashed black contour is the 24 to 28 m s^{-1} zonal isotachs. The thick dashed black solid contour in the right panels is the 100 m^2 s^{-2} contour of eddy available potential potential energy and the grey dots represent areas where the tendency of the eddy available potential energy is significant at the 90% level. The composites are plotted in 12 hour intervals from (a,f) t = -36 hours to (e,j) t = +12 hours.

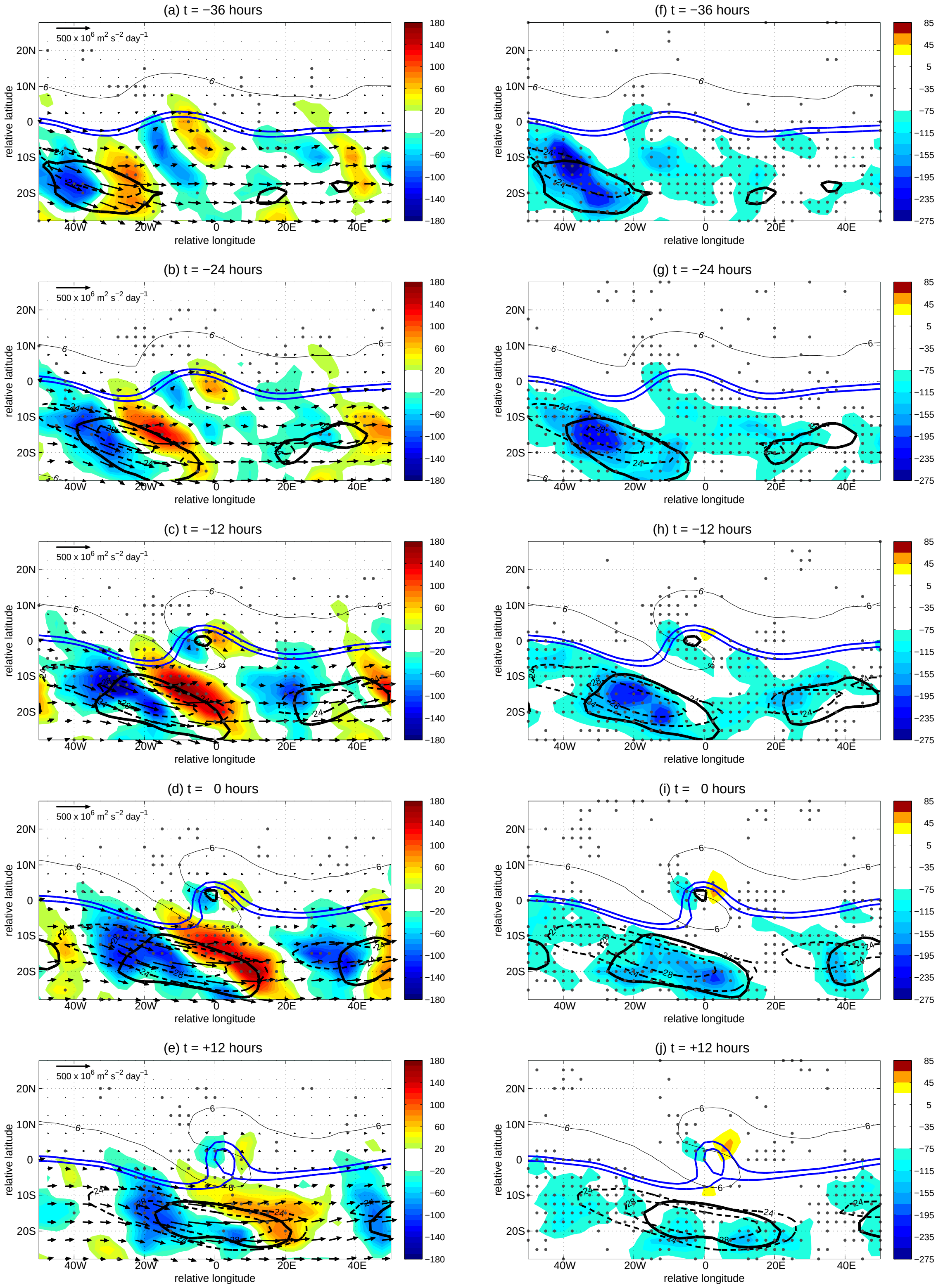

Figure 2: Time-lagged composites of eddy available potential energy fluxes $\mathbf{V}P_e$ (arrows) and their divergence ($-\nabla \cdot (\mathbf{V}P_e)$, shaded) in left panels and baroclinic conversion ($\omega\alpha$) shaded in the right panels, both plotted in m^2 s^{-2} day^{-1}. The blue contours, thin and thick dashed black contours and thick slid black contour and evolution time steps as in Fig. 1.

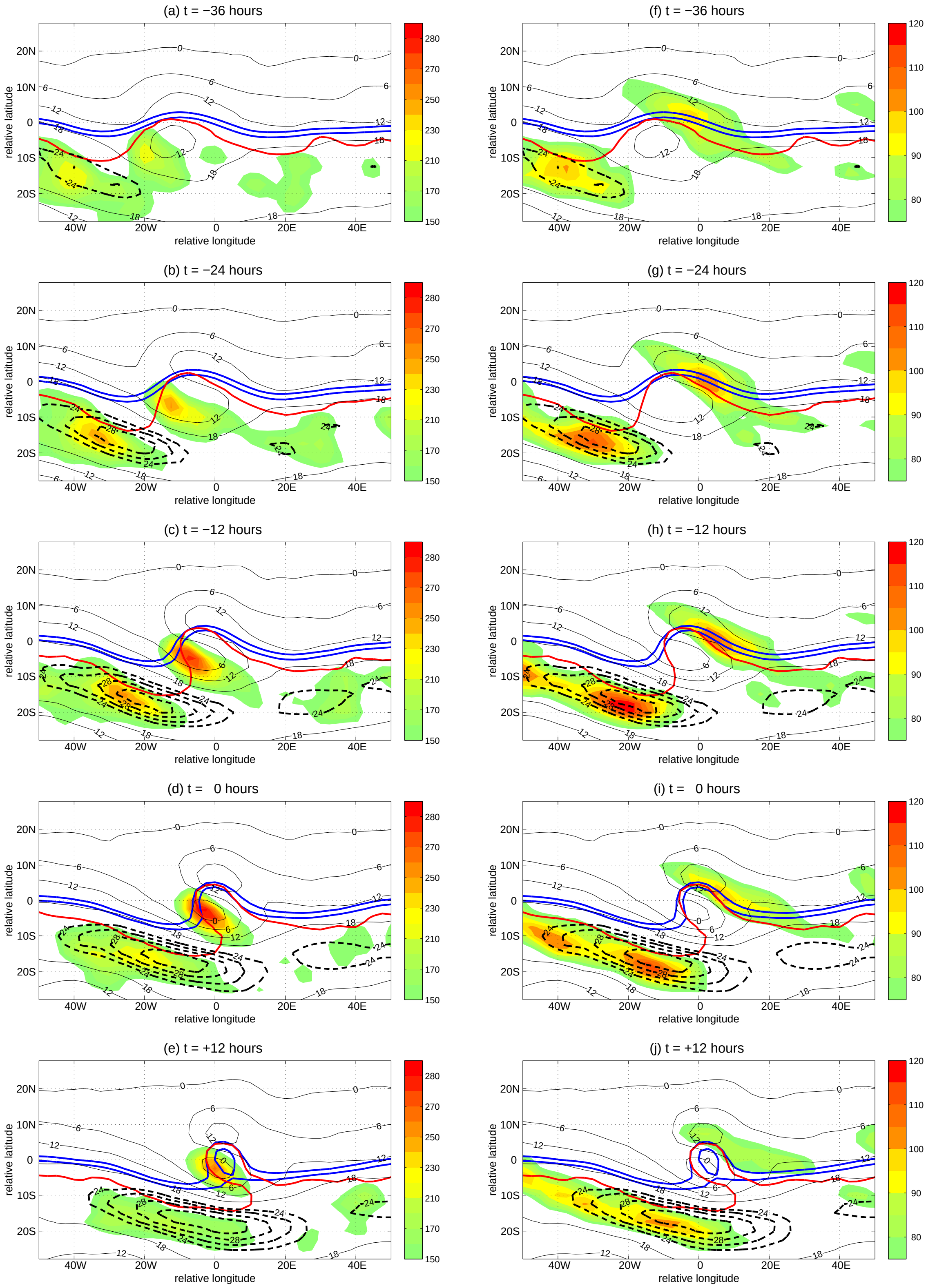

Figure 3: Time-lagged composites of K_e (shading on the left panels) and K_{BC} (shading on the right panels. The energy fields are plotted in m^2 s^{-2}. The blue contours, thin and thick dashed black contours, thick slid black contour and thick red contour and evolution time steps as in Fig. 1.

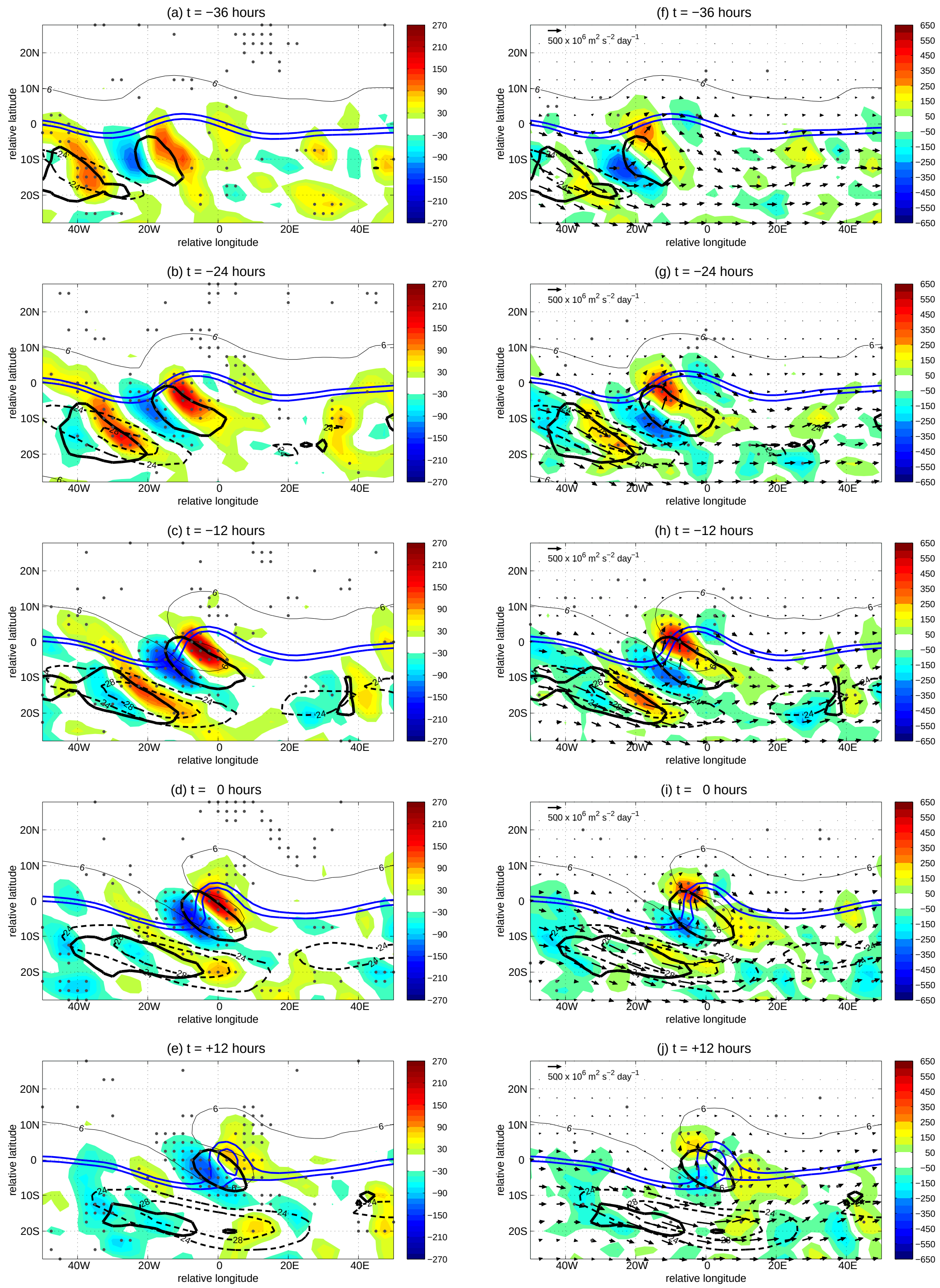

Figure 4: Time-lagged composites of $\partial_t K_e$ (shading on the left panels) and $\nabla \cdot (\mathbf{V} K_e)$ (shading on the right panels) and flux vectors $\mathbf{V} K_e$. The K_e tendency and the flux divergence are plotted in $\mathrm{m}^2\ \mathrm{s}^{-2}\ \mathrm{day}^{-1}$. The thick slid black contour is the 170 $\mathrm{m}^2\ \mathrm{s}^{-2}$. The blue contours, thin and thick dashed black contours and evolution time steps as in Fig. 1.

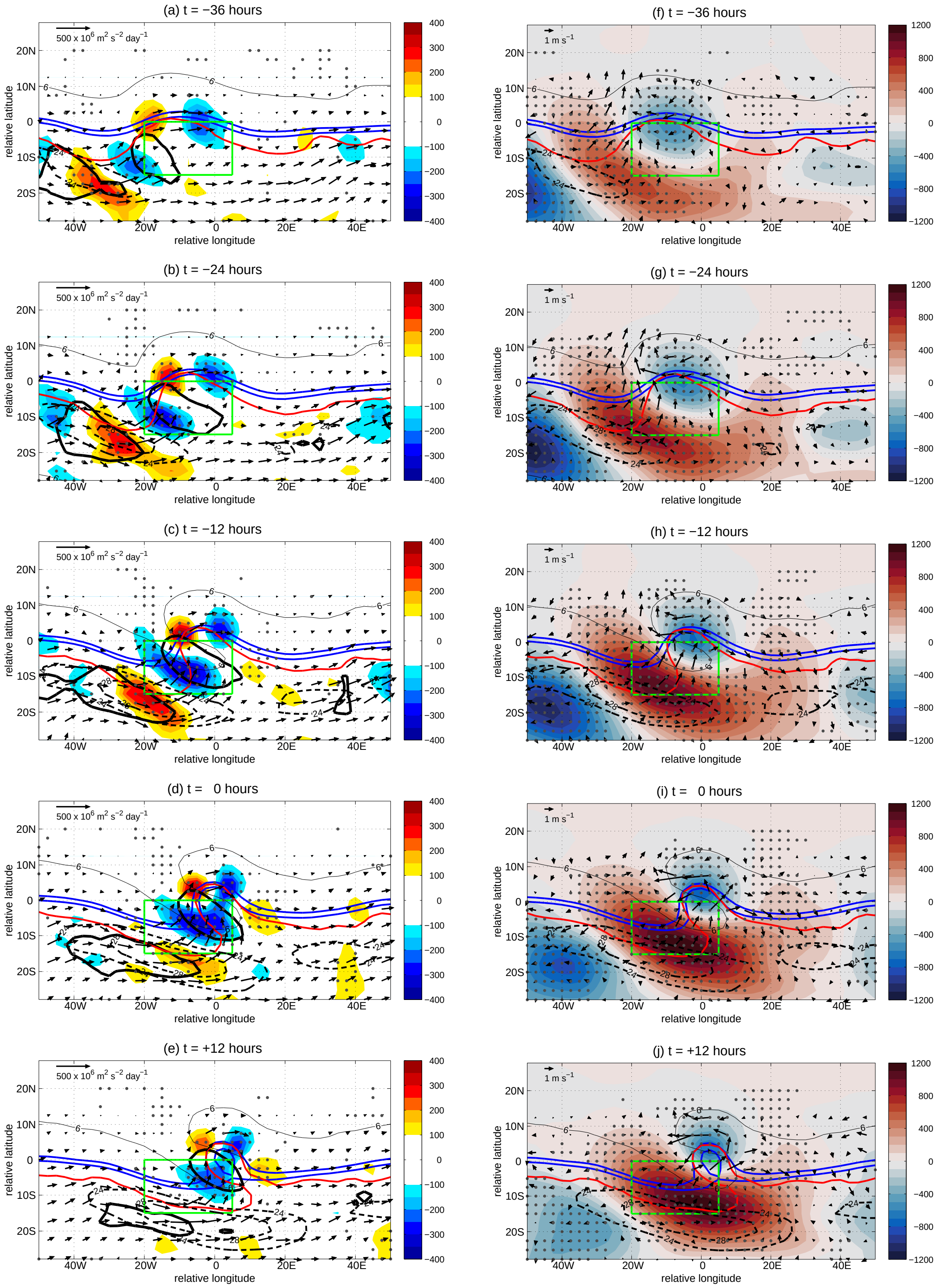

Figure 5: Time-lagged composites of $-\nabla\cdot\mathbf{v_a}\phi$ (shading on the left panels) and the arrows represent the ageostrophic geopotential flux $\mathbf{v}_a\phi = (\mathbf{v} - f^{-1}\mathbf{k}\times\nabla\phi)\phi$. The shading in the right panels represent ϕ and the arrows represent the ageostrophic flow $\mathbf{v}_a = u_a\mathbf{i} + v_a\mathbf{j}$. The thick slid black contour is the 170 m^2 s^{-2}. The blue contours, thin and thick dashed black contours, and thick red contour and evolution time steps as in Fig. 1.

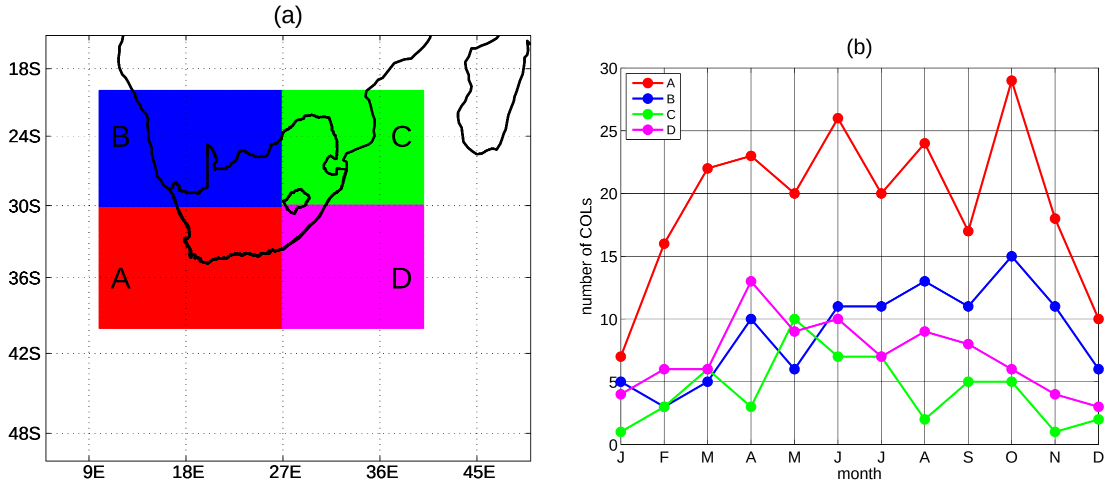

Figure 6: (a) South Africa divided into climatological regions A, B, C and D for COLs (Adapted from Singleton and Reason (2007). (b) Monthly variations of COLs for the regions in (a).

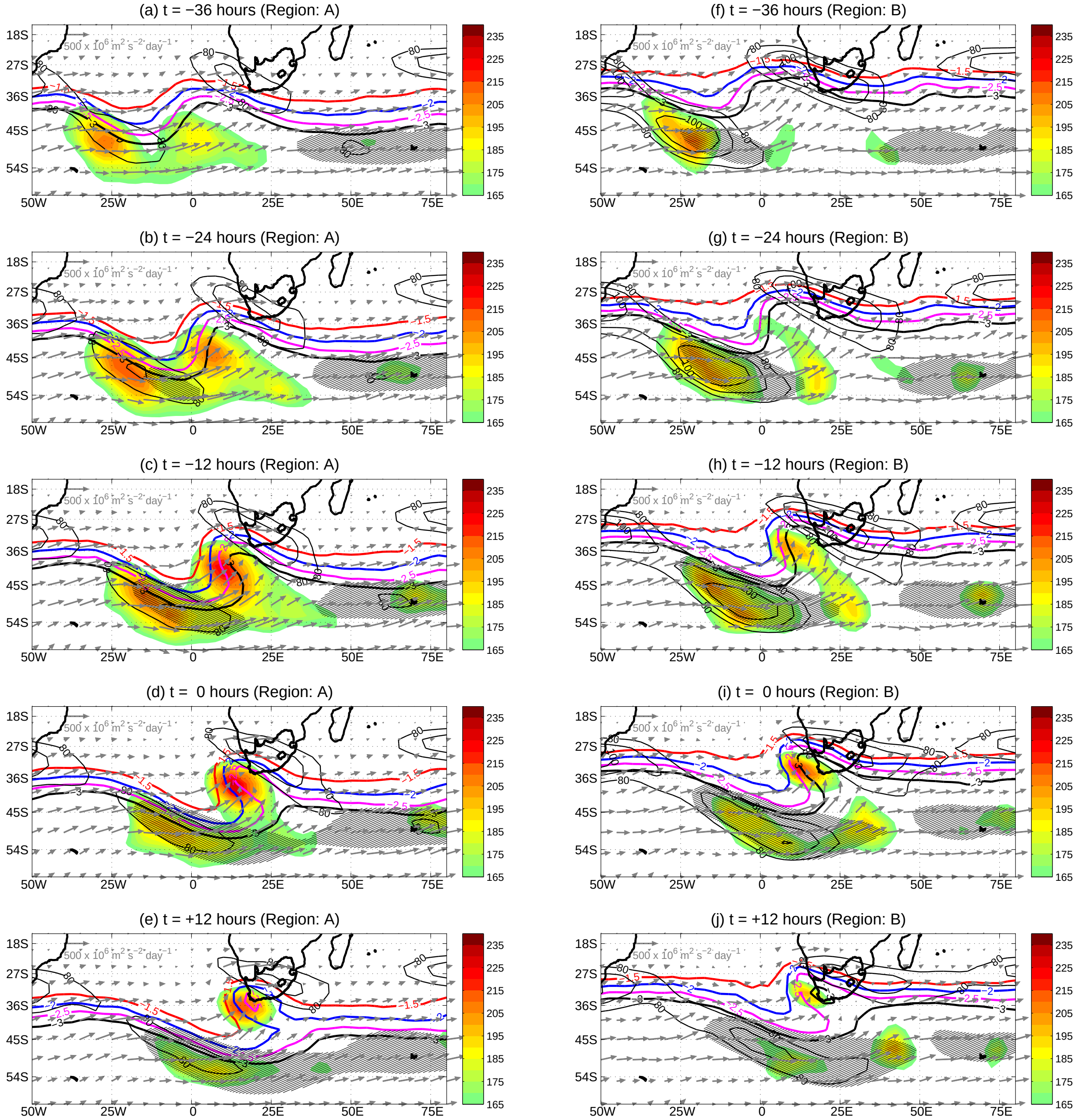

Figure 7: Time-lagged composites of eddy kinetic energy (dashed), zonal wind (25 m s^{-1} or greater hatched) and baroclinic kinetic energy (thin black contours). The kinetic energy is plotted in m^2 s^{-2}. The thick red, blue, magenta and black contours represent the -1.5, -2, -2.5 and -3 PVU contours, respectively, on the 330 K (left panels) and 340 K (right panels) isentropic surfaces. The arrows represent the ageostrophic geopotential fluxes as in Fig. 5. The left (right) panels are composites created using COLs whose initial points are in region A (B). Composites are plotted from (a, f) t = -36 hours to (e,j) t = +12 hours.

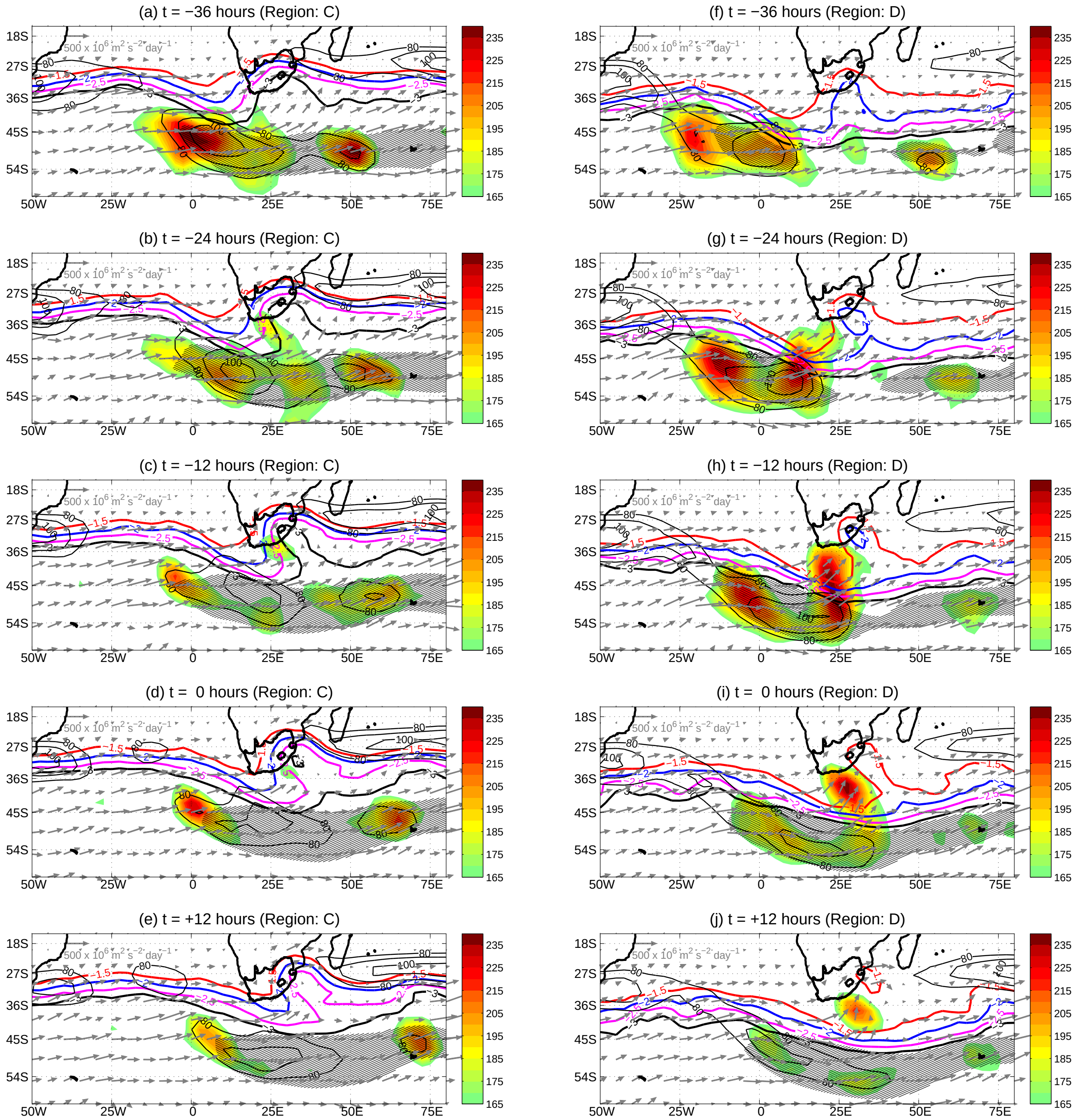

Figure 8: Same as Fig. 7 but for region C (D) on the left (right) panels. The PV on the left (right) panels is on the 340 (330) K isentropic surface.